



Ti₄O₇/g-C₃N₄ for Visible Light Photocatalytic Oxidation of Hypophosphite: Effect of Mass Ratio of Ti₄O₇/g-C₃N₄

Wei Guan¹, Zhenghua Zhang^{2*}, Shichao Tian^{3*} and Jianwei Du¹

¹ South China Institute of Environmental Sciences, The Ministry of Environment Protection of PRC, Guangzhou, China,

² Graduate School at Shenzhen, Research Institute of Environmental Engineering and Nano-Technology, Tsinghua University, Shenzhen, China, ³ Shenzhen Environmental Science and New Energy Technology Engineering Laboratory, Tsinghua-Berkeley Shenzhen Institute, Shenzhen, China

OPEN ACCESS

Edited by:

Fan Dong,
Chongqing Technology and Business
University, China

Reviewed by:

Guohong Wang,
Hubei Normal University, China
Aihua Xu,
Wuhan Textile University, China
Shaowen Cao,
Wuhan University of Technology,
China
Hongwei Huang,
China University of Geosciences,
China

*Correspondence:

Zhenghua Zhang
zhenghua.zhang@sz.tsinghua.edu.cn
Shichao Tian
18812672619@163.com

[†]These authors have contributed
equally to this work.

Specialty section:

This article was submitted to
Catalysis and Photocatalysis,
a section of the journal
Frontiers in Chemistry

Received: 07 May 2018

Accepted: 09 July 2018

Published: 24 July 2018

Citation:

Guan W, Zhang Z, Tian S and Du J
(2018) Ti₄O₇/g-C₃N₄ for Visible Light
Photocatalytic Oxidation of
Hypophosphite: Effect of Mass Ratio
of Ti₄O₇/g-C₃N₄ *Front. Chem.* 6:313.
doi: 10.3389/fchem.2018.00313

Hypophosphite wastewater treatment is still a critical issue in metallurgical processes and the oxidation of hypophosphite to phosphate followed by the precipitation of phosphate is an important strategy for hypophosphite wastewater treatment. Herein, Ti₄O₇/g-C₃N₄ photocatalysts with various mass ratios (Ti₄O₇ (m): g-C₃N₄ (m) = 0.5, 0.2, 0.1, and 0.05) were synthesized by a hydrolysis method and the effect of the mass ratio of Ti₄O₇ (m): g-C₃N₄ (m) on Ti₄O₇/g-C₃N₄ visible light photocatalytic oxidation of hypophosphite was evaluated. The as-prepared Ti₄O₇/g-C₃N₄ were characterized and confirmed by SEM, XPS, XRD and FTIR. Moreover, the specific surface area and the distribution of pore size of Ti₄O₇/g-C₃N₄ was also analyzed. Our results showed that Ti₄O₇/g-C₃N₄ exhibited remarkably improved photocatalytic performance on hypophosphite oxidation compared with g-C₃N₄ and meanwhile 1:2-Ti₄O₇/g-C₃N₄ with a mass ratio of 0.5 showed the best photocatalytic performance with the highest oxidation rate constant (17.7-fold and 91.0-fold higher than that of pure g-C₃N₄ and Ti₄O₇, respectively). The enhanced performance of photocatalytic oxidation of hypophosphite was ascribed to the heterojunction structure of Ti₄O₇/g-C₃N₄ with broader light absorption and significantly enhanced efficiency of the charge carrier (e⁻-h⁺) generation and separation. Additionally, the generated ·OH and ·O₂⁻ radicals contributed to the hypophosphite oxidation during the photocatalytic system.

Keywords: photocatalysts, hypophosphite oxidation, graphitic carbon nitride, sub-stoichiometric titanium oxides, visible light irradiation

INTRODUCTION

Hypophosphite wastewater is produced in metallurgical processes where hypophosphite is a widely used reducing reagent for chemical nickel deposition (Gan et al., 2007; Huang et al., 2009). The discharge of hypophosphite wastewater may result in eutrophication and therefore the further treatment is required (Piveteau et al., 2017; Tian et al., 2017). Coagulants such as Fe have been widely used for phosphorus removal (Shih et al., 2013), however, the hypophosphite precipitants are not stable due to the high solubility constant (Zhao et al., 2017). As such, the pre-oxidation of hypophosphite to phosphate is very important for hypophosphite wastewater treatment so as to facilitate the following precipitation of phosphate in the form of insoluble salts precipitates.

Photocatalysis is considered to be a useful technology for water treatment with advantages of energy-free by using solar energy and high oxidation efficiency of pollutants by hydroxyl radicals ($\cdot\text{OH}$) and superoxide radicals ($\cdot\text{O}_2^-$) generated during the photocatalytic process (Hao et al., 2017). The most commonly used TiO₂ photocatalyst, however, is greatly limited in wide applications especially under visible light or sunlight due to its main drawback of wide band gap (3.2 eV) (Hao et al., 2016; Ma et al., 2018). Therefore, photocatalysts with wide range of response wavelength as well as good photogenerated charge separation properties are urgently required for photocatalytic applications.

Recently, graphite-like carbon nitride (g-C₃N₄) has attracted lots of attentions due to its advantages including small band gap of 2.73 eV, robust chemical stability over a wide pH range of 0–14 (Zhang et al., 2014; Li et al., 2016a,b). Nevertheless, limitations including low surface area and poor photogenerated charge separation properties still hinder the photocatalytic applications of g-C₃N₄ (Shao et al., 2017). Preparation of g-C₃N₄-based heterojunction is an alternative pathway to facilitate the enhancement of charge separation and photocatalytic performance (Masih et al., 2017). For instance, photocatalysts with *p-n* junction exhibited excellent photocatalytic performance in environmental and energy applications (Huang et al., 2015a,b, 2016; Zhang et al., 2018).

Magnéli phase titanium suboxides (Ti_nO_{2n-1}) are substoichiometric titanium oxides, where *n* is an integer between 4 and 10 (i.e., 4, 5, 6, and 8) (Zaky and Chaplin, 2014). Among various compositions of Ti_nO_{2n-1}, Ti₄O₇ has the properties of best conductivity (1,500 S cm⁻¹) and the robust resistance to aggressive chemical conditions (Ganiyu et al., 2016). Construction of g-C₃N₄/Ti₄O₇ heterojunction significantly improved the photocatalytic performance as a result of the effective enhancement of charge separation was reported in our previous work (Guan et al., 2018). However, the effect of the mass ratio of Ti₄O₇ (m): g-C₃N₄ (m) of the g-C₃N₄/Ti₄O₇ heterojunction on photocatalytic performance is still unknown. In this study, the effect of the mass ratio of Ti₄O₇/g-C₃N₄ (Ti₄O₇ (m): g-C₃N₄ (m) = 0.5, 0.2, 0.1 and 0.05) on photocatalytic oxidation of hypophosphite was evaluated in view of the photocatalytic performance, optical and electrochemical properties as well as the contributions of $\cdot\text{OH}$ and $\cdot\text{O}_2^-$ radicals generated during the photocatalytic process. Our results indicated that Ti₄O₇/g-C₃N₄ with a mass ratio of 0.5 showed the highest rate constant of photocatalytic oxidation of hypophosphite (17.7-fold and 91.0-fold higher than that of pure g-C₃N₄ and Ti₄O₇, respectively).

MATERIALS AND METHODS

Chemicals

The reagents used for the preparation and performance characterization of g-C₃N₄/Ti₄O₇ were analytical grade and included sub-stoichiometric titanium oxide, melamine, urea, sodium hypophosphite, sodium sulfate, isopropanol, sodium

hydroxide, sulfuric acid. All chemicals were bought from Sinopharm Chemical Reagent Co., Ltd. (Beijing, China). In addition, all solutions were prepared using freshly prepared Milli-Q water (Millipore, 18.2 MΩ cm).

Preparation of Ti₄O₇/g-C₃N₄ Photocatalysts

Graphite-like carbon nitride was prepared first using a liquid-based growth method (Sun et al., 2018). Then, g-C₃N₄ (2 g) and Ti₄O₇ (1, 0.4, 0.2, 0.1 g) were well mixed in the 0.1 mol/L NaOH solution (100 mL) using ultrasonication following by the annealing procedure at 160°C for 20 h. Subsequently, the as-prepared g-C₃N₄/Ti₄O₇ with various mass ratios (Ti₄O₇ (m): g-C₃N₄ (m) = 0.5, 0.2, 0.1, and 0.05) were dried at 60°C for 12 h before usage and noted as 1:2-Ti₄O₇/g-C₃N₄, 1:5-Ti₄O₇/g-C₃N₄, 1:10-Ti₄O₇/g-C₃N₄ and 1:20-Ti₄O₇/g-C₃N₄, respectively.

Analysis and Test Methods

The as-prepared g-C₃N₄/Ti₄O₇ were characterized by scanning electron microscopy (SEM) (JEOL JSM-6701F), X-ray photoelectron spectroscopy (XPS) (Phi Quantern instrument with C 1s peak (284.8 eV) as the calibrated reference), X-ray diffraction (XRD) (model D/max RA, Rigaku Co., Japan), and fourier transforms infrared spectroscopy spectra (FTIR) (Bruker Tensor-27). The specific surface area and the pore size distribution of the as-prepared g-C₃N₄/Ti₄O₇ were calculated by Brunauer-Emmett-Teller (BET) equation and Barrett-Joyner-Halenda (BJH) method according to the N₂ adsorption/desorption isotherms. The optical and electrochemical properties of the as-prepared g-C₃N₄/Ti₄O₇ were evaluated by Ultraviolet-visible diffraction spectra (UV-vis DRS) (UV-2450, Shimadzu, Japan) and CHI 660B electrochemical system in view of photocurrent (PC), cyclic voltammetry (CV) and electrochemical impedance spectroscopy (EIS). The contributions of $\cdot\text{OH}$ and $\cdot\text{O}_2^-$ radicals generated during the visible light photocatalytic process were identified by comparing the efficiencies of hypophosphite oxidation in the absence and presence of isopropanol (IPA) and N₂ purging.

Analysis of Photocatalytic Performance

The photocatalytic performance of g-C₃N₄/Ti₄O₇ was characterized by photocatalytic oxidation of hypophosphite with the concentration of hypophosphite measured by ion chromatography using a 732 IC detector. A metal-halide lamp (35 W, Philips) with the light strength of ~5 mW cm⁻² was used as the light source and a UV-cutoff filter of 420 nm was used to provide the visible light with the wavelength over 420 nm. Before the photocatalytic experiments, g-C₃N₄/Ti₄O₇ with various mass ratios (10 mg) dispersed in 100 mg L⁻¹ hypophosphite aqueous solution (100 mL) were continuously stirred for 30 min in the dark to achieve the adsorption-desorption equilibrium. After that, the visible light photocatalytic oxidation of hypophosphite was conducted with the above solutions exposing to the visible light irradiation and sampling conducted at 1 h intervals over

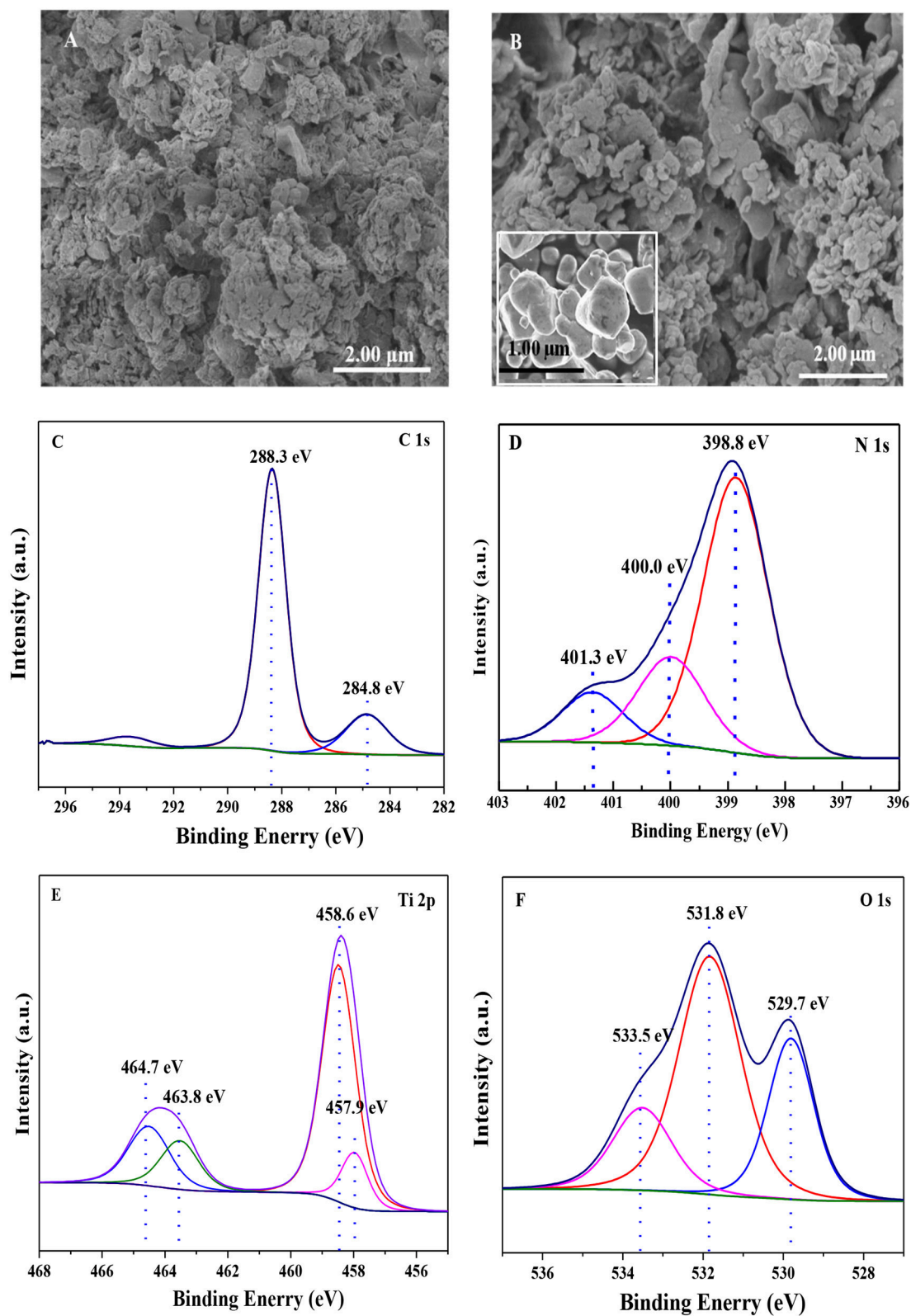
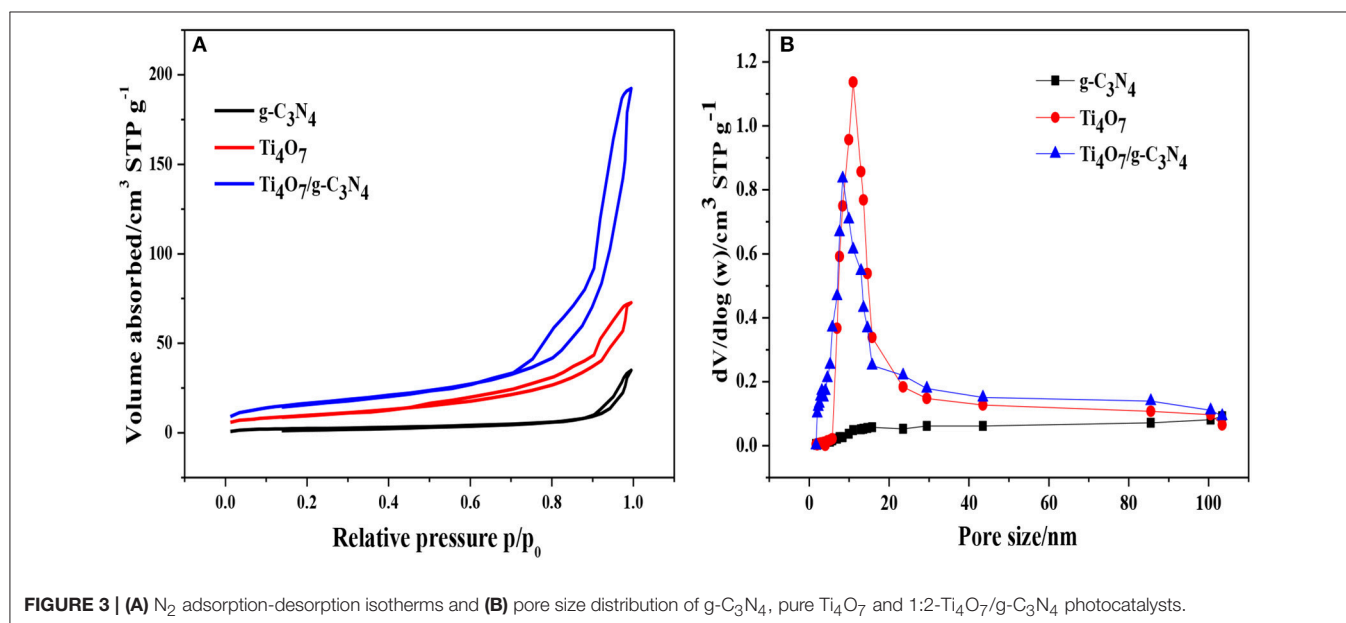
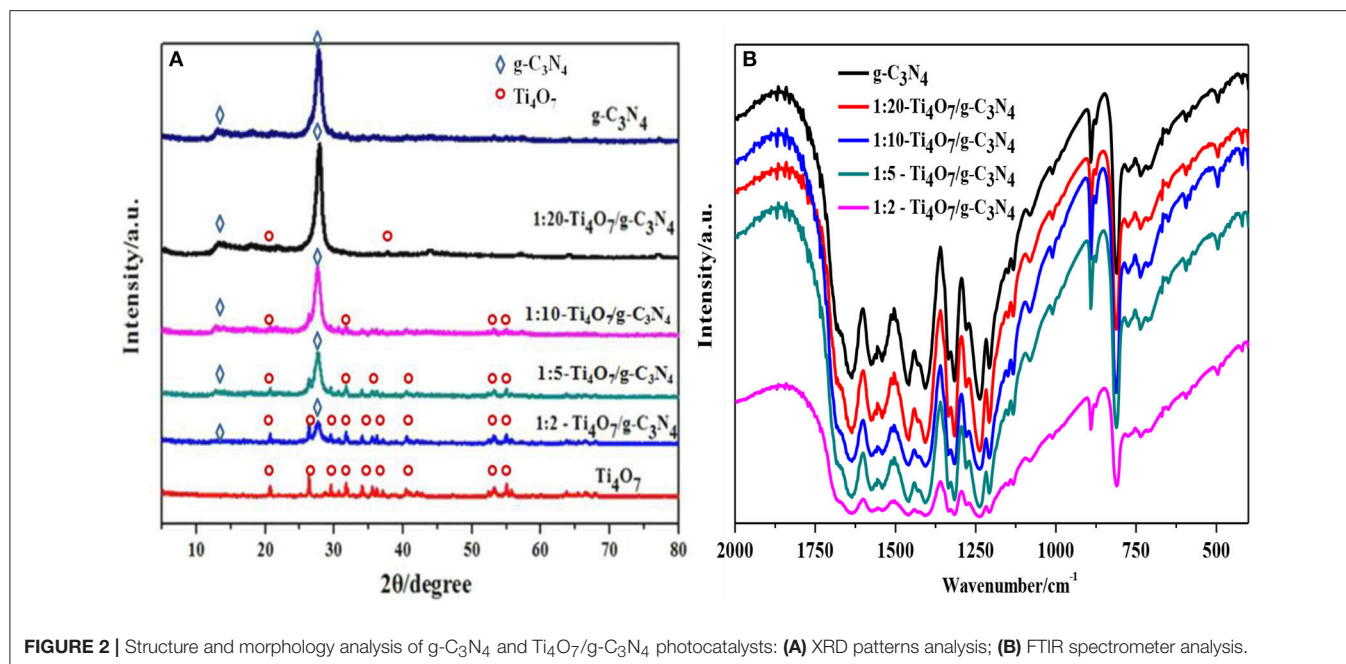


FIGURE 1 | The SEM images of (A) g-C₃N₄, (B) Ti₄O₇/g-C₃N₄ photocatalysts; and XPS spectrum of (C) C 1s, (D) N 1s, (E) Ti 2p, (F) O 1s of Ti₄O₇/g-C₃N₄ photocatalyst.



6 h experimental period. More detailed information about the photocatalytic experiment can be found in our most recent paper (Guan et al., 2018). The oxidation efficiency of hypophosphite (η) was calculated using the following equation (Guan et al., 2017):

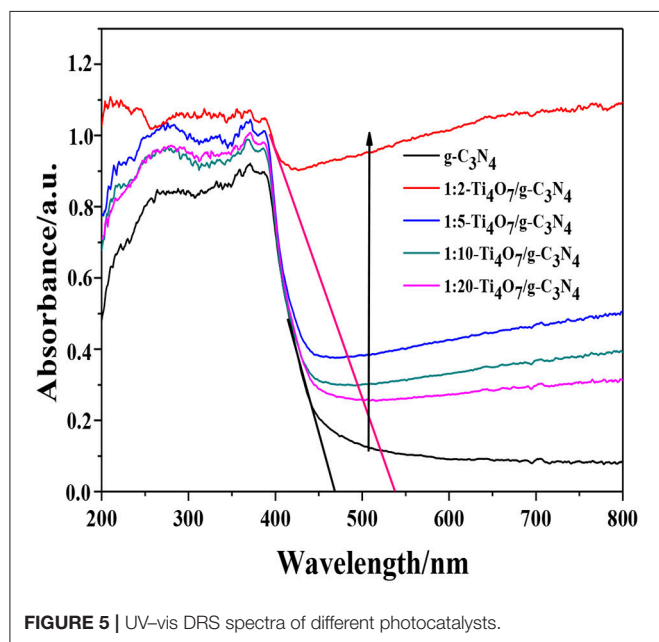
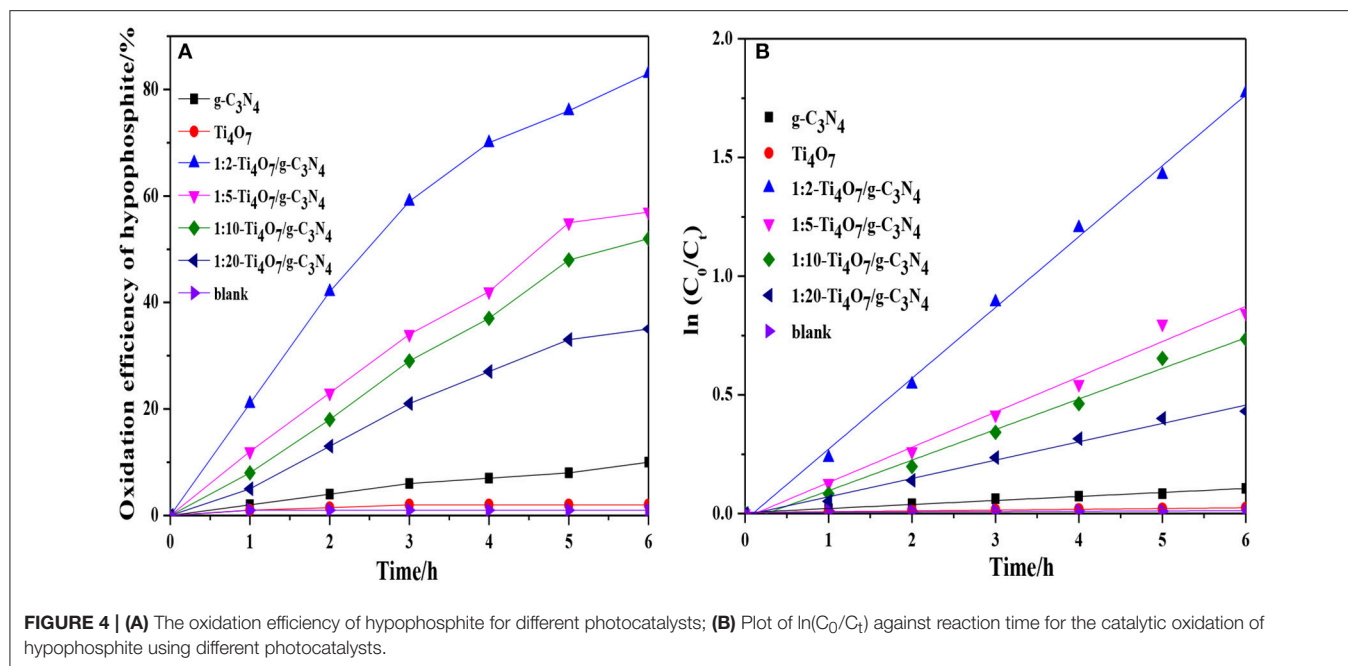
$$\eta = \frac{C_0 - C_t}{C_0} \times 100\% \quad (1)$$

where C_0 and C_t represent the concentrations of hypophosphite at initial and given time, respectively.

RESULTS AND DISCUSSION

Materials Characterization

The SEM images of pure g-C₃N₄ and Ti₄O₇/g-C₃N₄ photocatalysts were shown in **Figure 1** that g-C₃N₄ had a sheet-like structure (**Figure 1A**) and spheroidal Ti₄O₇ crystals were deposited on the surface of C₃N₄ (**Figure 1B**). The corresponding XPS high resolution spectra of Ti₄O₇/g-C₃N₄ were analyzed as shown in **Figure 1**. There were two components for the XPS spectra of C 1s core level (**Figure 1C**), the standard reference carbon (284.8 eV) and the sp² bonded C in N=C(-N)₂ (288.3 eV) (Jo and Natarajan, 2015). With regard to the N 1s

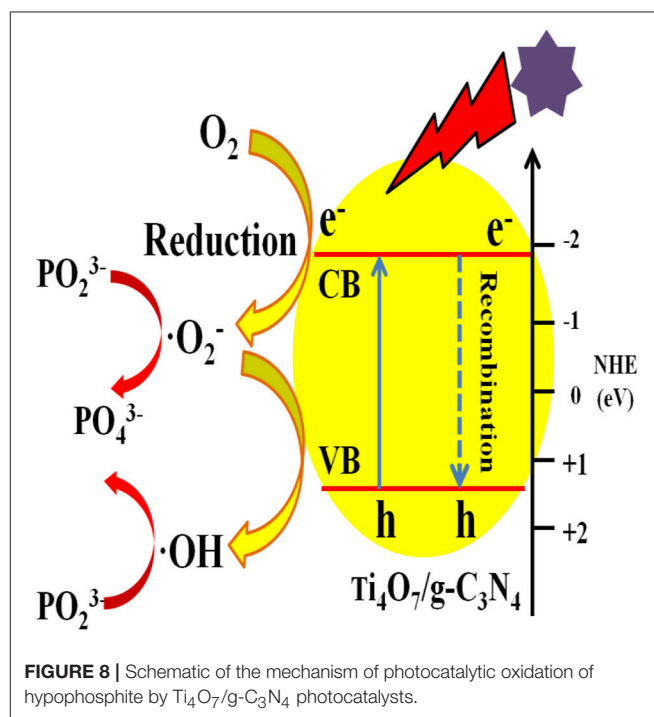
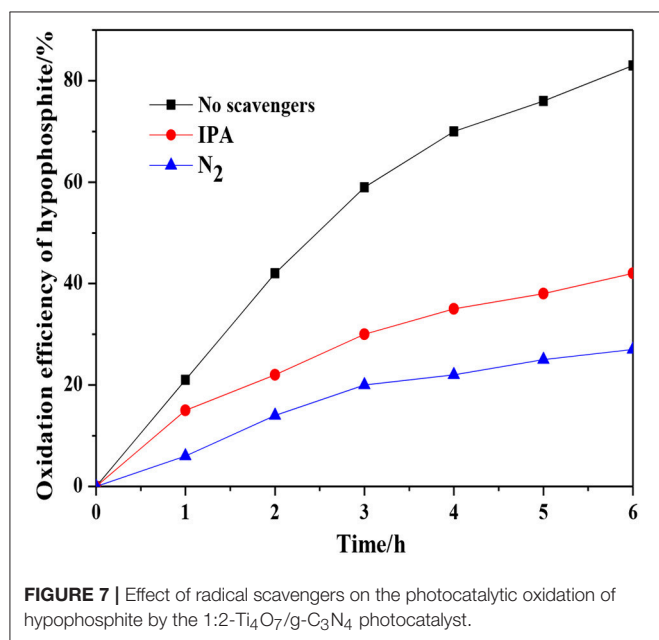
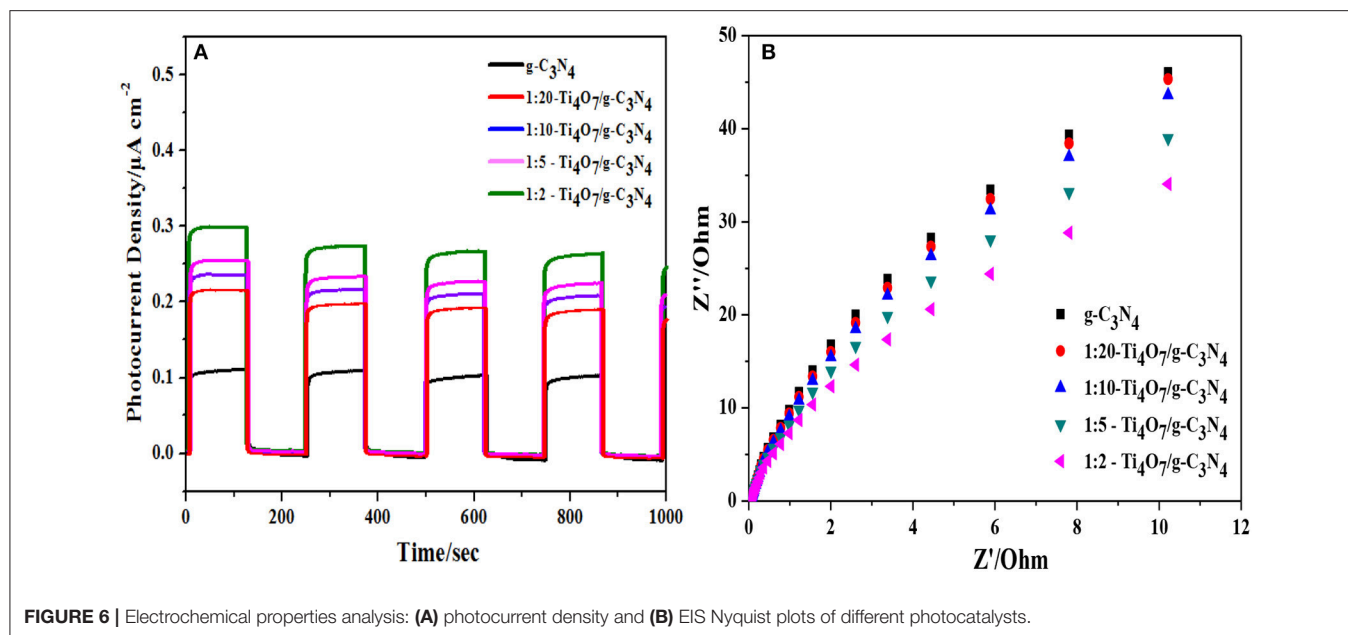


spectra, there were three peaks (**Figure 1D**), the main peak at 398.8 eV assigned to sp^2 nitrogen (C=N-C) involved in triazine rings, the peak at 400.0 eV originated from the tertiary nitrogen bonded to carbon atoms in the form of N-(C)₃ (Wu et al., 2013) and the peak at 401.3 eV ascribed to amino functions (C-N-H) (Gao et al., 2014). These assignments of C 1s and N 1s were agreed well with the XPS results of g-C₃N₄ reported previously. Meanwhile, Ti₄O₇ is a mixed-valence compound with two evenly occupied Ti⁴⁺ ($3d^0$) and Ti³⁺ ($3d^1$) configurations. Four peaks were observed for Ti 2p spectra (**Figure 1E**) that two broad peaks

at 458.6 eV and 464.7 eV were respectively assigned to Ti 2p_{1/2} and Ti 2p_{3/2} peaks of Ti⁴⁺, and another two peaks at 457.9 eV and 463.8 eV were assigned to Ti³⁺ (Zeng et al., 2017). In terms of the O 1s spectra, three peaks were observed (**Figure 1F**) that the peak at 533.5 eV was assigned to the C-O functional groups, and the peaks at 531.8 and 529.7 eV were ascribed to the OH-Ti and O-Ti bonds (Li et al., 2017). The XPS results confirmed the presence of Ti₄O₇ on the surface of g-C₃N₄ with covalent bonds.

The XRD phase structures of Ti₄O₇/g-C₃N₄ photocatalysts with various mass ratios were shown in **Figure 2A**. Peaks at 13.10° and 27.40° were indexed as (1 0 0) plane of tri-s-triazine units and (0 0 2) plane of the conjugated aromatic system of g-C₃N₄, respectively (Liang and Zhu, 2016). Meanwhile, major peaks of Ti₄O₇ including 20.7, 26.3, 29.5, 31.7, 34.0, 36.3, 40.5, 53.1, 55.0, 63.8, and 66.4° were also found (Guo et al., 2016). With increase of the mass ratio of Ti₄O₇ (m): g-C₃N₄ (m), the intensity of the Ti₄O₇ peaks became stronger while that of the C₃N₄ peaks became weaker. Furthermore, Ti₄O₇/g-C₃N₄ especially 1:2-Ti₄O₇/g-C₃N₄ (mass ratio of Ti₄O₇/g-C₃N₄ of 0.5) matched well with the reference of pure Ti₄O₇ and g-C₃N₄, indicating that the main structures of Ti₄O₇ and g-C₃N₄ were not destroyed during the synthesis process of Ti₄O₇/g-C₃N₄.

The as-prepared Ti₄O₇/g-C₃N₄ photocatalysts with various mass ratios were further characterized by FTIR as shown in **Figure 2B**. Typical absorption peaks of 1,230–1,630 cm⁻¹ were attributed to tri-s-triazine ring moieties of g-C₃N₄. For example, the absorption peaks of 1,638 and 1,570 cm⁻¹ were related to C=N stretching, and the peaks of 1,474, 1,410, 1,322, 1,241 cm⁻¹ were attributed to C-N stretching. Meanwhile, the sharp peak of 810 cm⁻¹ was due to the bending vibration of heptazine rings, indicating that the heptazine units might exist in C₃N₄ (Hatamie et al., 2018). With increase of the mass ratio of Ti₄O₇/g-C₃N₄, the absorption intensity related to the vibrational bands



of g-C₃N₄ became weaker. The presence of Ti₄O₇ in Ti₄O₇/g-C₃N₄ restricted the evolution trend of g-C₃N₄ and thus alleviated the severe stacking of aromatic units of g-C₃N₄. Additionally, the delocalized π - π conjugated electronic system of g-C₃N₄ facilitated the transfer of photogenerated electron-hole pairs during the photocatalytic process (Jourshabani et al., 2018).

The nitrogen adsorption-desorption isotherms and pore size distribution of pure Ti₄O₇, g-C₃N₄ and 1:2-Ti₄O₇/g-C₃N₄ photocatalysts were shown in Figure 3. The specific surface area calculated according to Figure 3A was 116.0,

56.5, and 174.0 m²·g⁻¹ for Ti₄O₇, g-C₃N₄ and 1:2-Ti₄O₇/g-C₃N₄, respectively. Generally, a catalyst with larger surface area could offer more active sites for adsorption and photodegradation toward organic pollutants, resulting in an enhanced photodecomposition activity (Dong et al., 2015). As such, compared with pure Ti₄O₇ and g-C₃N₄, 1:2-Ti₄O₇/g-C₃N₄ with larger specific surface area would facilitate photocatalytic oxidation of hypophosphite. Moreover, the pore size distribution of 1:2-Ti₄O₇/g-C₃N₄ was between 5

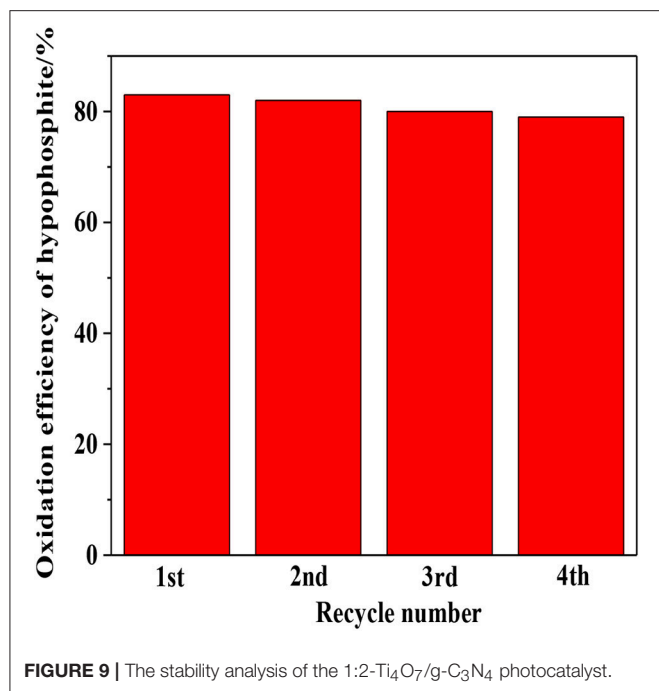


FIGURE 9 | The stability analysis of the 1:2-Ti₄O₇/g-C₃N₄ photocatalyst.

and 15 nm and that of pure Ti₄O₇ was mainly in the range of 10–25 nm, while no obvious mesopores were observed for g-C₃N₄ (Figure 3B).

Photocatalytic Performance Analysis

The photocatalytic performance of different photocatalysts was analyzed and compared as shown in Figure 4A. Ti₄O₇/g-C₃N₄ exhibited the significantly improved efficiency in hypophosphite oxidation under visible light irradiation ($\lambda > 420$ nm) in comparison to the pure g-C₃N₄ and Ti₄O₇. Additionally, the oxidation efficiency of hypophosphite was increased with increase of the mass ratio of Ti₄O₇/g-C₃N₄ and 1:2-Ti₄O₇/g-C₃N₄ illustrated the best photocatalytic performance with the highest oxidation efficiency of 83.6%. Furthermore, the photocatalytic oxidation reaction of hypophosphite was well fitted by pseudo first-order kinetic ($R^2 > 0.95$) as shown in Figure 4B and the rate constant of 1:2-Ti₄O₇/g-C₃N₄ was 17.7-fold and 91.0-fold higher than that of pure g-C₃N₄ and Ti₄O₇, respectively. The low efficiency of photocatalytic oxidation of hypophosphite for pure g-C₃N₄ was possibly because of the rapid combination of electron-hole pairs (Yan et al., 2018). Similarly, the photocatalytic performance of pure Ti₄O₇ was extremely limited herein, which was mainly due to the wide band gap of 2.9 eV of pure Ti₄O₇ (Maragatha et al., 2017). Nevertheless, the efficiency of photocatalytic oxidation of hypophosphite was remarkably improved especially for 1:2-Ti₄O₇/g-C₃N₄ possibly as a result of the Ti₄O₇/g-C₃N₄ heterojunction with effectively increased recombination lifetime of electron-hole pairs and better charge transfer during the photocatalytic process, which was discussed in the following parts.

Optical Properties Analysis

Generally, the band gap of a semiconductor is related to its photocatalytic performance, because it determines the absorption properties of the incident photon, the recombination lifetime of the electron-hole pairs and transfer of charge carriers. As shown in Figure 5, Ti₄O₇/g-C₃N₄ showed a distinct red-shift in comparison to pure g-C₃N₄ in the UV-vis diffuse reflectance spectra. Moreover, the absorption intensities ranging from 450 to 800 nm gradually strengthened with increase of the mass ratio of Ti₄O₇ (m): g-C₃N₄ (m), indicating that the Ti₄O₇/g-C₃N₄ heterojunction with good interaction between Ti₄O₇ and g-C₃N₄ facilitated the enhancement of visible-light harvesting (Chang et al., 2018). The band gap of Ti₄O₇/g-C₃N₄ was determined such that (Ai et al., 2018):

$$(\alpha h\nu)^2 = A(h\nu - E_g) \quad (2)$$

where α is the optical absorption coefficient; h is the Planck's constant; ν is the photonic frequency; A is the proportionality constant; E_g is the band gap.

The band gap followed the order: 1:2-Ti₄O₇/g-C₃N₄ (2.07 eV) < 1:5-Ti₄O₇/g-C₃N₄ (2.25 eV) < 1:10-Ti₄O₇/g-C₃N₄ (2.33 eV) < 1:20-Ti₄O₇/g-C₃N₄ (2.43 eV) < pure g-C₃N₄ (2.70 eV). As such, the narrowed band gap of Ti₄O₇/g-C₃N₄ would effectively enhance the photoabsorption efficiency, which thus contributed to the improved efficiency of photocatalytic oxidation of hypophosphite as shown in Figure 4.

Electrochemical Properties Analysis

CV and EIS results can indicate the combination efficiency of electron-hole pairs during the photocatalytic process. As shown in Figure 6A, the transient photoelectrochemical response current density of Ti₄O₇/g-C₃N₄ increased with the increase of the mass ratio of Ti₄O₇/g-C₃N₄. 1:2-Ti₄O₇/g-C₃N₄ had the highest photocurrent density of 0.30 $\mu\text{A cm}^{-2}$, while the photocurrent density for pure g-C₃N₄ was only 0.10 $\mu\text{A cm}^{-2}$. The enlarged photocurrent density of Ti₄O₇/g-C₃N₄ suggested the more efficient charge carrier (e^- - h^+) generation on the Ti₄O₇/g-C₃N₄ surface (Liu et al., 2017). Herein, the electrons in the valence band of g-C₃N₄ were excited upon visible light irradiation and then migrated to the conduction band of Ti₄O₇ with effectively enhanced efficiency of the charge carrier (e^- - h^+) generation and separation (Samanta and Srivastava, 2017), which improved the photocatalytic performance as indicated in Figure 4. In addition, the photoelectrochemical response current density of Ti₄O₇/g-C₃N₄ switched reversibly and was unchanged after repetitive ON/OFF illumination cycles, indicating the good photoelectrochemical stability of Ti₄O₇/g-C₃N₄.

Charge transfer of photocatalysts is another very important factor determining the photocatalytic performance (Kang et al., 2016). EIS was applied to analyze the photogenerated electron transfer process of Ti₄O₇/g-C₃N₄. As shown in Figure 6B, the arc radius decreased gradually with increase of the mass ratio of Ti₄O₇/g-C₃N₄ and the arc radius was lowest for 1:2-Ti₄O₇/g-C₃N₄. It is well known that the radius of Nyquist circle is related to the interfacial charge transfer that the smaller radius of Nyquist circle indicates a faster interfacial charge transfer and

lower recombination rate of electron and hole (Guo et al., 2017). Herein, the decreased arc radius of Ti₄O₇/g-C₃N₄ indicated that 1:2-Ti₄O₇/g-C₃N₄ in comparison to pure g-C₃N₄ would also facilitate the photocatalytic oxidation of hypophosphite as evident in **Figure 4**.

Proposed Mechanism

Reactive oxygen species (ROS) including $\cdot\text{O}_2^-$ and $\cdot\text{OH}$ would be generated during the photocatalytic system (Huang et al., 2017a,b). Herein, the contributions of $\cdot\text{OH}$ and $\cdot\text{O}_2^-$ to the photocatalytic oxidation of hypophosphite were analyzed by evaluation of the photocatalytic oxidation efficiency of hypophosphite in the presence of isopropanol (IPA) acting as the scavenger of $\cdot\text{OH}$ (Tian et al., 2015) and N₂ purging applied to reduce the superoxide $\cdot\text{O}_2^-$ radicals (Zhang et al., 2017). As shown in **Figure 7**, the oxidation efficiency of hypophosphite was decreased to 42 and 27% in the presence of IPA and N₂, respectively. In contrast, that value was 83% without radical scavengers. These results indicated that $\cdot\text{OH}$ and $\cdot\text{O}_2^-$ radicals significantly contributed to the photocatalytic oxidation of hypophosphite and other radicals such as singlet oxygen (¹O₂) and peroxy (RO₂·) may also make a contribution as evident by the lowest efficiency of 27% rather than 0% (Huang et al., 2017a).

The photocatalytic mechanism of Ti₄O₇/g-C₃N₄ was proposed as shown in **Figure 8**. Under visible light irradiation, electrons in the valence band of g-C₃N₄ were excited and then the excited electrons migrated to the conduction band of Ti₄O₇ through the heterojunction surface of Ti₄O₇/g-C₃N₄ with the generation of holes in the valence band of g-C₃N₄ (Zhu et al., 2018). The electrons on the surface of Ti₄O₇ could easily react with O₂ adsorbed on the Ti₄O₇/g-C₃N₄ surface to generate $\cdot\text{O}_2^-$ radicals for hypophosphite oxidation. Meanwhile, the active $\cdot\text{OH}$ radicals with high redox potential were generated through $\cdot\text{O}_2^-$ radicals, which further facilitated the oxidation of hypophosphite (Nosaka and Nosaka, 2017; Guan et al., 2018). Therefore, it can be concluded that the oxidation of hypophosphite was mainly ascribed to $\cdot\text{OH}$ and $\cdot\text{O}_2^-$ radicals generated during the photocatalytic process as shown in **Figure 8**.

Analysis of Stability

The stability of photocatalyst is another vital consideration to evaluate the photocatalytic performance. As shown in **Figure 9**,

relatively robust reusability was exhibited by 1:2-Ti₄O₇/g-C₃N₄ photocatalyst that the efficiency of photocatalytic oxidation of hypophosphite was almost stable in the range of 79–84% after four repetitive experiments. The slight decrease of oxidation efficiency was possibly due to the inevitable mass loss of photocatalyst during the recycling process.

CONCLUSION

In this work, Ti₄O₇/g-C₃N₄ with various mass ratios (Ti₄O₇ (m): g-C₃N₄ (m) = 0.5, 0.2, 0.1, and 0.05) were synthesized by a hydrolysis method and the effect of the mass ratio of Ti₄O₇/g-C₃N₄ on Ti₄O₇/g-C₃N₄ visible light photocatalytic oxidation of hypophosphite was evaluated. Ti₄O₇/g-C₃N₄ exhibited remarkably improved photocatalytic performance on hypophosphite oxidation in comparison to pure g-C₃N₄ and 1:2-Ti₄O₇/g-C₃N₄ with a mass ratio of 0.5 showed the best photocatalytic performance with the highest oxidation rate constant of photocatalytic (17.7-fold and 91.0-fold higher than that of pure g-C₃N₄ and Ti₄O₇, respectively). The heterojunction structure of Ti₄O₇/g-C₃N₄ with broader light absorption significantly enhanced the efficiency of the charge carrier (e⁻-h⁺) generation and separation. $\cdot\text{OH}$ and $\cdot\text{O}_2^-$ radicals generated during the photocatalytic process were the main radicals contributing to the oxidation of hypophosphite.

AUTHOR CONTRIBUTIONS

WG: experiment. ZZ: paper writing. ST: data analysis. JD: sample analysis.

FUNDING

This work was supported by National Natural Science Foundation of China (No. 51608086); Science and Technology Planning Project of Guangdong Province (2017A050506032); Science and Technology Project from Chongqing (CSTC2015JCYJA20027); Chongqing Key Laboratory of Environmental Materials and Remediation Technology, Chongqing University of Arts and Sciences (CKE1407); Scientific Research Foundation of Chongqing University of Arts and Sciences (R2014CH08).

REFERENCES

- Ai, Z. Z., Zhao, G., Zhong, Y. Y., Shao, Y. L., Huang, B. B., Wu, Y. Z., et al. (2018). Phase junction CdS: High efficient and stable photocatalyst for hydrogen generation. *Appl. Catal. B: Environ.* 221, 179–186. doi: 10.1016/j.apcatb.2017.09.002
- Chang, F., Zheng, J. J., Wang, X. F., Xu, Q., Deng, B. Q., Hu, X. F., et al. (2018). Heterojunctioned non-metal binary composites silicon carbide/g-C₃N₄ with enhanced photocatalytic performance. *Mat. Sci. Semicon. Proc.* 75, 183–192. doi: 10.1016/j.mssp.2017.11.043
- Dong, G. H., Ho, W. K., Li, Y. H., and Zhang, L. Z. (2015). Facile synthesis of porous graphene-like carbon nitride (C₆N₉H₃) with excellent photocatalytic activity for NO removal. *Appl. Catal. B: Environ.* 174–175, 477–485. doi: 10.1016/j.apcatb.2015.03.035
- Gan, X. P., Wu, Y. T., Liu, L., Shen, B., and Hu, W. B. (2007). Electroless copper plating on PET fabrics using hypophosphite as reducing agent. *Surf. Coat. Tech.* 201, 7018–7023. doi: 10.1016/j.surfcoat.2007.01.006
- Ganiyu, S. O., Oturan, N., Raffy, S., Cretin, M., Esmilaire, R., van Hullebusch, E. et al. (2016). Sub-stoichiometric titanium oxide (Ti₄O₇) as a suitable ceramic anode for electrooxidation of organic pollutants: a case study of kinetics, mineralization and toxicity assessment of amoxicillin. *Water Res.* 106, 171–182. doi: 10.1016/j.watres.2016.09.056
- Gao, D. Q., Xu, Q., Zhang, J., Yang, Z. L., Si, M. S., Yan, Z. J., et al. (2014). Defect-related ferromagnetism in ultrathin metal-free g-C₃N₄ nanosheets. *Nanoscale* 6, 2577–2581. doi: 10.1039/c3nr04743a
- Guan, W., Sun, G. G., Yin, L., Zhang, Z. H., and Tian, S. C. (2018). Ti₄O₇/g-C₃N₄ visible light photocatalytic performance on hypophosphite oxidation: effect of annealing temperature. *Front. Chem.* 6:37. doi: 10.3389/fchem.2018.00037

- Guan, W., Tian, S. C., Cao, D., Chen, Y. T., and Zhao, X. (2017). Electrooxidation of nickel-ammonia complexes and simultaneous electrodeposition recovery of nickel from practical nickel-electroplating rinse wastewater. *Electrochim. Acta* 246, 1230–1236. doi: 10.1016/j.electacta.2017.06.121
- Guo, L., Jing, Y., and Chaplin, B. P. (2016). Development and characterization of ultrafiltration TiO₂ magnéli phase reactive electrochemical membranes. *Environ. Sci. Technol.* 50, 1428–1436. doi: 10.1021/acs.est.5b04366
- Guo, W., Wang, J. Y., Fan, C., Chen, Z., Liu, P., Zhu, D. J., et al. (2017). Synthesis of carbon self-repairing porous g-C₃N₄ nanosheets/NiCo₂S₄ nanoparticles hybrid composite as high-performance electrode materials for supercapacitors. *Electrochim. Acta* 253, 68–77. doi: 10.1016/j.electacta.2017.09.025
- Hao, R. R., Wang, G. H., Jiang, C. J., Tang, H., and Xu, Q. C. (2017). *In situ* hydrothermal synthesis of g-C₃N₄/TiO₂ heterojunction photocatalysts with high specific surface area for rhodamine B degradation. *Appl. Surf. Sci.* 411, 400–410. doi: 10.1016/j.apsusc.2017.03.197
- Hao, R. R., Wang, G. H., Tang, H., Sun, L. L., Xu, C., and Han, D. Y. (2016). Template-free preparation of macro/mesoporous g-C₃N₄/TiO₂ heterojunction photocatalysts with enhanced visible light photocatalytic activity. *Appl. Catal. B: Environ.* 187, 47–58. doi: 10.1016/j.apcatb.2016.01.026
- Hatamie, A., Marahel, F., and Sharifat, A. (2018). Green synthesis of graphitic carbon nitride nanosheet (g-C₃N₄) and using it as a label-free fluorosensor for detection of metronidazole via quenching of the fluorescence. *Talanta* 176, 518–525. doi: 10.1016/j.talanta.2017.08.059
- Huang, H. W., Han, X., Li, X. W., Wang, S. C., Chu, P. K., and Zhang, Y. H. (2015a). Fabrication of multiple heterojunctions with tunable visible-light-active photocatalytic reactivity in BiOBr–BiOI full-range composites based on microstructure modulation and band structures. *ACS Appl. Mater. Interfaces* 7, 482–492. doi: 10.1021/am5065409
- Huang, H. W., He, Y., Du, X., Chu, P. K., and Zhang, Y. H. (2015b). A general and facile approach to heterostructured core/shell BiVO₄/BiOI *p-n* junction: room-temperature *in situ* assembly and highly boosted visible-light photocatalysis. *ACS Sustainable Chem. Eng.* 3, 3262–3273. doi: 10.1021/acsschemeng.5b01038
- Huang, H. W., Tu, S. C., Zeng, C., Zhang, T. R., Reshak, A. H., and Zhang, Y. H. (2017a). Macroscopic polarization enhancement promoting photo- and piezoelectric-induced charge separation and molecular oxygen activation. *Angew. Chem. Int. Ed.* 56, 11860–11864. doi: 10.1002/anie.201706549
- Huang, H. W., Xiao, K., He, Y., Zhang, T. R., Dong, F., Du, X., et al. (2016). *In situ* assembly of BiOI@Bi₁₂O₁₇C₁₂ *p-n* junction: charge induced unique front-lateral surfaces coupling heterostructure with high exposure of BiOI {001} active facets for robust and nonselective photocatalysis. *Appl. Catal. B: Environ.* 199, 75–86. doi: 10.1016/j.apcatb.2016.06.020
- Huang, H. W., Xiao, K., Tian, N., Dong, F., Zhang, T. R., Du, X., et al. (2017b). Template-free precursor-surface-etching route to porous, thin g-C₃N₄ nanosheets for enhancing photocatalytic reduction and oxidation activity. *J. Mater. Chem. A* 5, 17452–17463. doi: 10.1039/c7ta04639a
- Huang, Y. H., Su, H. T., and Lin, L. W. (2009). Removal of citrate and hypophosphite binary components using fenton, photo-fenton and electro-fenton processes. *J. Environ. Sci.* 21, 35–40. doi: 10.1016/S1001-0742(09)60008-5
- Jo, W. K., and Natarajan, T. S. (2015). Influence of TiO₂ morphology on the photocatalytic efficiency of direct Z-scheme g-C₃N₄/TiO₂ photocatalysts for isoniazid degradation. *Chem. Eng. J.* 281, 549–565. doi: 10.1016/j.cej.2015.06.120
- Jourshabani, M., Shariatinia, Z., and Badiie, A. (2018). Synthesis and characterization of novel Sm₂O₃/S-doped g-C₃N₄ nanocomposites with enhanced photocatalytic activities under visible light irradiation. *Appl. Surf. Sci.* 427, 375–387. doi: 10.1016/j.apsusc.2017.08.051
- Kang, K., Watanabe, S., Broch, K., Sepe, A., Brown, A., Nasrallah, I., et al. (2016). 2D coherent charge transport in highly ordered conducting polymers doped by solid state diffusion. *Nat. Mater.* 15, 896–902. doi: 10.1038/NMAT4634
- Li, Y. A., Wang, M. Q., Bao, S. J., Lu, S. Y., Xu, M. W., Long, D. B., et al. (2016b). Tuning and thermal exfoliation graphene-like carbon nitride nanosheets for superior photocatalytic activity. *Ceram. Int.* 42, 18521–18528. doi: 10.1016/j.ceramint.2016.08.190
- Li, Y., Zhang, C., Shuai, D. M., Naraginti, S., Wang, D. W., and Zhang, W. L. (2016a). Visible-light-driven photocatalytic inactivation of MS2 by metal-free g-C₃N₄: virucidal performance and mechanism. *Water Res.* 106, 249–258. doi: 10.1016/j.watres.2016.10.009
- Li, Z. Q., Qi, M. Y., Tu, C. Y., Wang, W. P., Chen, J. R., and Wang, A. J. (2017). Highly efficient removal of chlorotetracycline from aqueous solution using graphene oxide/TiO₂ composite: properties and mechanism. *Appl. Surf. Sci.* 425, 765–775. doi: 10.1016/j.apsusc.2017.07.027
- Liang, F. F., and Zhu, Y. F. (2016). Enhancement of mineralization ability for phenol via synergetic effect of photoelectrocatalysis of g-C₃N₄ film. *Appl. Catal. B: Environ.* 180, 324–329. doi: 10.1016/j.apcatb.2015.05.009
- Liu, Q., Chen, T. X., Guo, Y. R., Zhang, Z. G., and Fang, X. M. (2017). Grafting Fe(III) species on carbon nanodots/Fe-doped g-C₃N₄ via interfacial charge transfer effect for highly improved photocatalytic performance. *Appl. Catal. B: Environ.* 205, 173–181. doi: 10.1016/j.apcatb.2016.12.028
- Ma, L. N., Wang, G. H., Jiang, C. J., Bao, H. L., and Xu, Q. C. (2018). Synthesis of core-shell TiO₂@g-C₃N₄ hollow microspheres for efficient photocatalytic degradation of rhodamine B under visible light. *Appl. Surf. Sci.* 430, 263–272. doi: 10.1016/j.apsusc.2017.07.282
- Maragatha, J., Rani, C., Rajendran, S., and Karuppuchamy, S. (2017). Microwave synthesis of nitrogen doped Ti₄O₇ for photocatalytic applications. *Physica. E* 93, 78–82. doi: 10.1016/j.physe.2017.05.020
- Masih, D., Ma, Y. Y., and Rohani, S. (2017). Graphitic C₃N₄ based noble-metal-free photocatalyst systems: a review. *Appl. Catal. B: Environ.* 206, 556–588. doi: 10.1016/j.apcatb.2017.01.061
- Nosaka, Y., and Nosaka, A. Y. (2017). Generation and detection of reactive oxygen species in photocatalysis. *Chem. Rev.* 117, 11302–11336. doi: 10.1021/acs.chemrev.7b00161
- Piveteau, S., Picard, S., Dabert, P., and Daumer, M. L. (2017). Dissolution of particulate phosphorus in pig slurry through biological acidification: a critical step for maximum phosphorus recovery as struvite. *Water Res.* 124, 693–701. doi: 10.1016/j.watres.2017.08.017
- Samanta, S., and Srivastava, R. (2017). Thermal catalysis vs. photocatalysis: a case study with FeVO₄/g-C₃N₄ nanocomposites for the efficient activation of aromatic and benzylic CH bonds to oxygenated products. *Appl. Catal. B: Environ.* 218, 621–636. doi: 10.1016/j.apcatb.2017.06.043
- Shao, H. X., Zhao, X., Wang, Y. B., Mao, R., Wang, Y., Qiao, M., et al. (2017). Synergetic activation of peroxymonosulfate by Co₃O₄ modified g-C₃N₄ for enhanced degradation of diclofenac sodium under visible light irradiation. *Appl. Catal. B: Environ.* 218, 810–818. doi: 10.1016/j.apcatb.2017.07.016
- Shih, Y. J., Lin, C. P., and Huang, Y. H. (2013). Application of fered-fenton and chemical precipitation process for the treatment of electroless nickel plating wastewater. *Sep. Purif. Technol.* 104, 100–105. doi: 10.1016/j.seppur.2012.11.025
- Sun, X., Jiang, D., Zhang, L., and Wang, W. Z. (2018). Alkaline modified g-C₃N₄ photocatalyst for high selective oxide coupling of benzyl alcohol to benzoin. *Appl. Catal. B: Environ.* 220, 553–560. doi: 10.1016/j.apcatb.2017.08.057
- Tian, Q., Zhuang, L. J., Ong, S. K., Wang, Q., Wang, K. W., Xie, X. H., et al. (2017). Phosphorus (P) recovery coupled with increasing influent ammonium facilitated intracellular carbon source storage and simultaneous aerobic phosphorus & nitrogen removal. *Water Res.* 119, 267–275. doi: 10.1016/j.watres.2017.02.050
- Tian, S. C., Li, Y. B., and Zhao, X. (2015). Cyanide removal with a copper/active carbon fiber cathode via a combined oxidation of a fenton-like reaction and *in situ* generated copper oxides at anode. *Electrochim. Acta* 180, 746–755. doi: 10.1016/j.electacta.2015.09.006
- Wu, G. S., Thind, S. S., Wen, J. L., Yan, K., and Chen, A. C. (2013). A novel nanoporous α-C₃N₄ photocatalyst with superior high visible light activity. *Appl. Catal. B: Environ.* 142–143, 590–597. doi: 10.1016/j.apcatb.2013.05.070
- Yan, X. X., Jia, Z. Y., Che, H. B., Chen, S. Q., Hu, P., Wang, J. S., et al. (2018). A selective ion replacement strategy for the synthesis of copper doped carbon nitride nanotubes with improved photocatalytic hydrogen evolution. *Appl. Catal. B: Environ.* 234, 19–25. doi: 10.1016/j.apcatb.2018.04.020
- Zaky, A. M., and Chaplin, B. P. (2014). Mechanism of *p*-substituted phenol oxidation at a Ti₄O₇ reactive electrochemical membrane. *Environ. Sci. Technol.* 48, 5857–5867. doi: 10.1021/es5010472
- Zeng, X. K., Wang, Z. Y., Wang, G., Gengenbach, T. R., McCarthy, D. T., Deletic, A., et al. (2017). Highly dispersed TiO₂ nanocrystals and WO₃ nanorods

- on reduced graphene oxide: Z-scheme photocatalysis system for accelerated photocatalytic water disinfection. *Appl. Catal. B: Environ.* 218, 163–173. doi: 10.1016/j.apcatb.2017.06.055
- Zhang, F. W., Wen, Q. J., Hong, M. Z., Zhuang, Z. Y., and Yu, Y. (2017). Efficient and sustainable metal-free GR/C₃N₄/CDots ternary heterostructures for versatile visible-light-driven photoredox applications: toward synergistic interaction of carbon materials. *Chem. Eng. J.* 307, 593–603. doi: 10.1016/j.cej.2016.08.120
- Zhang, L. P., Wang, G. H., Xiong, Z. Z., Tang, H., and Jiang, C. J. (2018). Fabrication of flower-like direct Z-scheme β-Bi₂O₃/g-C₃N₄ photocatalyst with enhanced visible light photoactivity for rhodamine B degradation. *Appl. Surf. Sci.* 436, 162–171. doi: 10.1016/j.apsusc.2017.11.280
- Zhang, X. S., Hu, J. Y., and Jiang, H. (2014). Facile modification of a graphitic carbon nitride catalyst to improve its photoreactivity under visible light irradiation. *Chem. Eng. J.* 256, 230–237. doi: 10.1016/j.cej.2014.07.012
- Zhao, Z. L., Dong, W. Y., Wang, H. J., Chen, G. H., Wang, W., Liu, Z. K., et al. (2017). Advanced oxidation removal of hypophosphite by O₃/H₂O₂ combined with sequential Fe(II) catalytic process. *Chemosphere* 180, 48–56. doi: 10.1016/j.chemosphere.2017.04.003
- Zhu, Z., Huo, P. W., Lu, Z. Y., Yan, Y. S., Liu, Z., Shi, W. D., et al. (2018). Fabrication of magnetically recoverable photocatalysts using g-C₃N₄ for effective separation of charge carriers through like-Z-scheme mechanism with Fe₃O₄ mediator. *Chem. Eng. J.* 331, 615–625. doi: 10.1016/j.cej.2017.08.131

Conflict of Interest Statement: The authors declare that the research was conducted in the absence of any commercial or financial relationships that could be construed as a potential conflict of interest.

Copyright © 2018 Guan, Zhang, Tian and Du. This is an open-access article distributed under the terms of the Creative Commons Attribution License (CC BY). The use, distribution or reproduction in other forums is permitted, provided the original author(s) and the copyright owner(s) are credited and that the original publication in this journal is cited, in accordance with accepted academic practice. No use, distribution or reproduction is permitted which does not comply with these terms.